J. Min. Metall. Sect. B-Metall. 59 (2) (2023) 231 - 241

Journal of Mining and Metallurgy, Section B: Metallurgy

MODELING OF PARTIAL REDUCTION OF HEMATITE WITH CARBON-MONOXIDE IN TUNNEL FURNACE

S. Salimibani, A. Jafari-Ramiani, S. Firoozi

Amirkabir University of Technology (Tehran Polytechnic), Faculty of Materials and Metallurgical Engineering, Tehran, Iran

(Received 29 November 2022; Accepted 07 August 2023)

Abstract

DRI production in tunnel furnaces sometimes encounters an incomplete degree of reduction. A model is required to tackle heterogeneous reaction rates, crucible heat transfer, and oxide morphology. Herein, a three-phase model is proposed based on the heat and mass conservation and reaction kinetics, to describe the reduction of hematite to magnetite in the crucibles. The model was implemented via a Fortran program using finite volume discretization, and the results were validated against available experimental data. The model moderated the uncertainties in the reaction rate with a reformulation considering the solid morphology. The results also revealed that the speed and diameter of the crucible have dominant effects on the overall progress of the reduction by changing the heat transfer rate within the crucible. In contrast, the crucible thickness has a minor effect on the reaction and could be regarded as an economical parameter.

Keywords: *Multiphase Modeling; Hematite; Direct Reduction; Kinetics; Ironmaking*

1. Introduction

Direct-Reduction-Iron comprises ~110 Mton (~5%) of total iron produced globally. In the reactor of the process, pellets of iron oxide are heated up to 800-1200 ℃ and exposed to a reducing gas like CO, H_2, or natural gas to produce sponge iron. Using tunnel furnaces, e.g., in Hoganas technology [1-4], it has become feasible to eliminate the pelletizing process and to reduce low-grade iron concentrates [5] and secondary iron oxides with a small-scale investment. A sponge iron tunnel kiln has three regions: pre-heating, firing, and cooling. Rail-traveling wagons enter the tunnel, carrying columns of cylindrical containers (silicon carbide crucibles or clay saggers). The crucibles contain concentric iron oxides, coal, and lime powder layers. Flowing backward, the internal atmospheric air, which has been warmed up in the third zone, reaches a temperature of 1100-1200 °C by burning natural gas in the firing region. The entering crucibles are exposed to hot air and warm up the contained materials. The coal fines gradually produce a carbon monoxide atmosphere inside the cylinders [6]. Then, the reducing gas consumes oxygen in the structure of iron oxides. The product is supposed to be a porous iron structure, which is then cooled in the third region of the tunnel.

Attempts have been carried out to quantify the progress of the reduction of iron oxides in tunnel kilns. Temperature distribution, fuel consumption, heat loss, and heat storage in an iron production kiln were evaluated by Yu [13] to obtain a proper range of gas flow rates to save energy. Adequate and controlled circulation of hot air in the furnace has been prescribed as a key attribute to enhancing the thermal efficiency of the process [14]. Donskoi, et al. [15] considered the reduction of iron oxide as a first-order chemical reaction to model the kinetics of the process. Several studies have been carried out to evaluate the activation energy of the reduction of hematite. A glance at the values has been presented in Table 1. Donskoi and Mcelwain [16] developed a mathematical model consisting of equations for iron ore reduction (hematite-magnetite-wustite-iron), coal consumption, and heat transfer. Seaton, et al. [17] modeled the reduction of iron ore composite powder. Gao, et al. [18] indicated that the gas-solid direct reduction processes were capable of using alternative resourses of iron ore. They studied the reduction kinetics of limonite pellets with different reducing gases. Pintowantoro, et al. [19] pointed out the effects of binder materials on the progress of the reduction and morphology of the product. Khattoi and Roy [20] examined the carbon and energy efficiencies of different configurations of the materials (composition, form, and stacking) in the containers of a pilot tunnel kiln. They revealed that the configuration of charged materials and the container considerably affected the

Corresponding author: sohrab.salimi@aut.ac.ir

https://doi.org/10.2298/JMMB221129020S

Table 1. *Reported activation energies for the reduction of hematite to magnetite*

References	Reactants	Activation energy
		E_A (kJ/mol)
Hou, et al. [7]	Fe_2O_3 / 5%CO-Ar	75.4
Colombo, et al. [8]	Fe_2O_3 / 100% H_2	108.7
Jozwiak, et al. [9]	Fe_2O_3 / 5% CO-Ar	70
Piotrowski, et al. [10]	Fe_2O_3 / 5.7%CO + 4.3% H_2-N_2	58.13
Pineau, et al. [11]	Fe_2O_3 / 10% H_2-N_2	75.9–114.1
Gaviria, et al. [12]	Fe_2O_3 / 5% H_2-Ar	94–102

efficiency of the reduction process. Abdul, et al. [21] investigated the effect of the dimensions of the iron oxide briquettes on the degree of metallization in the reduction process. They showed that the dimensions of input materials significantly influenced the diffusivity of reducing gas, and hence it affected the yield of the final product. Saleem, et al. [22] modeled the reduction kinetics of iron ore with a set of ODEs conjugated with a genetic algorithm. Haghi, et al. [23] proposed a model, describing the reduction of hematite-magnetite concentrate by graphite-calcium carbonate, to optimize the energy efficiency of the process. Yu, et al. [24] investigated the kinetics of the reduction isothermally on a laboratory scale. Valipour [25] showed that the reduction of magnetite regularly started after the reduction of hematite was completed. Therefore, it can be assumed that no other reaction took place simultaneously with the reduction of hematite to magnetite.

Although previous studies have shed some light on the details of the physics of the process, there are still ambiguities around the kinetic models of the gas-solid heterogeneous reactions and their rate constants [26]. The present study has focused on that issue and reassessed the mathematical formulation of the kinetics of the reduction. A multiphase model was proposed describing the tunnel kiln process with heat transfer, mass conservation of the species, and a kinetic coupling for a gas-solid heterogeneous hematite reduction in the radial direction of the crucibles. The reduction of hematite was considered partial, i.e., hematite to magnetite only, because the multiphase model had to be checked for a single heterogeneous reaction to eliminate the uncertainties and ensure that it predicted the conversion of the species correctly. In addition, the fact that the conversion of hematite to magnetite occurred almost without any other reaction interference provided more reliable data on a single heterogeneous reaction to validate the model. The following section describes the problem's details and the proposed mathematical formulation. Then, the model was implemented to predict how the reaction would proceed through different thermal regions of the furnace. The numerical results obtained from the model were demonstrated, evaluated, and discussed.

2. Problem identification

A tunnel kiln is considered with length L with three regions; the preheating L_1, the firing L_2, and the cooling. The problem concerns a single crucible with an internal radius of r_C and a thickness of d_C containing hematite and carbon fines and passing through the tunnel. The carbon fines consume oxygen and generate a mixture gas of carbon monoxide and carbon dioxide via the Boudouard reaction when the temperature reaches above ~700 K, i.e., CO_2+C↔CO. It is assumed that a certain ratio of CO-CO_2 mixture has been produced and taken as an input in the problem. Our focus is, however, on the next heterogeneous gas-solid reaction when hematite particles are reduced to magnetite according to the:

$$\begin{aligned} &CO_{(g)} + 3Fe_2O_{3\,(s)} \rightarrow CO_{2\,(g)} + 2Fe_3O_{4\,(s)} \\ &Z_A A_{(1)} + Z_B B_{(2)} \rightarrow Z_C C_{(1)} + Z_D D_{(3)} \end{aligned} \quad (1)$$

The thermodynamics of the above reaction gives the total Gibbs free energy of $\Delta G_0 \approx$ *-44304 - 50.29T* (J/mol) in the temperature range of 298-1642 K [27, 28]. The problem requires obtaining transient distributions of temperature and variations of the fractions of the species within the crucible. It is also desired to find how the reduction progress is affected by changing the crucible's thickness and radius.

Assumptions have been made to describe the problem mathematically: (1) Variations are ignored along the angular and vertical directions of the crucibles; (2) In comparison to the heat flow rates by radiation, convection, and conduction in the crucible, the rate of generation/consumption of heat due to the chemical reactions is negligible; (3) The furnace air temperature is assumed to have a piece-wise linear regime in each furnace zone; (4) The coal fines have already produced carbon monoxide within the crucible, i.e., a constant concentration of the reducing gas is available; (5) The rate of transport of the carbon monoxide through the pores of the material is about

two orders higher than the diffusion rate of the oxygen anions and ferrous cations through the solid structure of iron oxides. The reduction of iron oxides is supposed to be controlled by the diffusion of ions in solid materials [10, 24]. Therefore, it is assumed that the concentration of carbon monoxide is kept constant in the gas phase according to the ratio of input material.

3. Mathematical model

3.1. Computational Domain

Figure 1 illustrates the computational domain of the problem. The materials consist of three phases; gas mixtures (phase 1 including two species A: CO and C: CO_2), hematite (phase 2), and magnetite (phase 3).

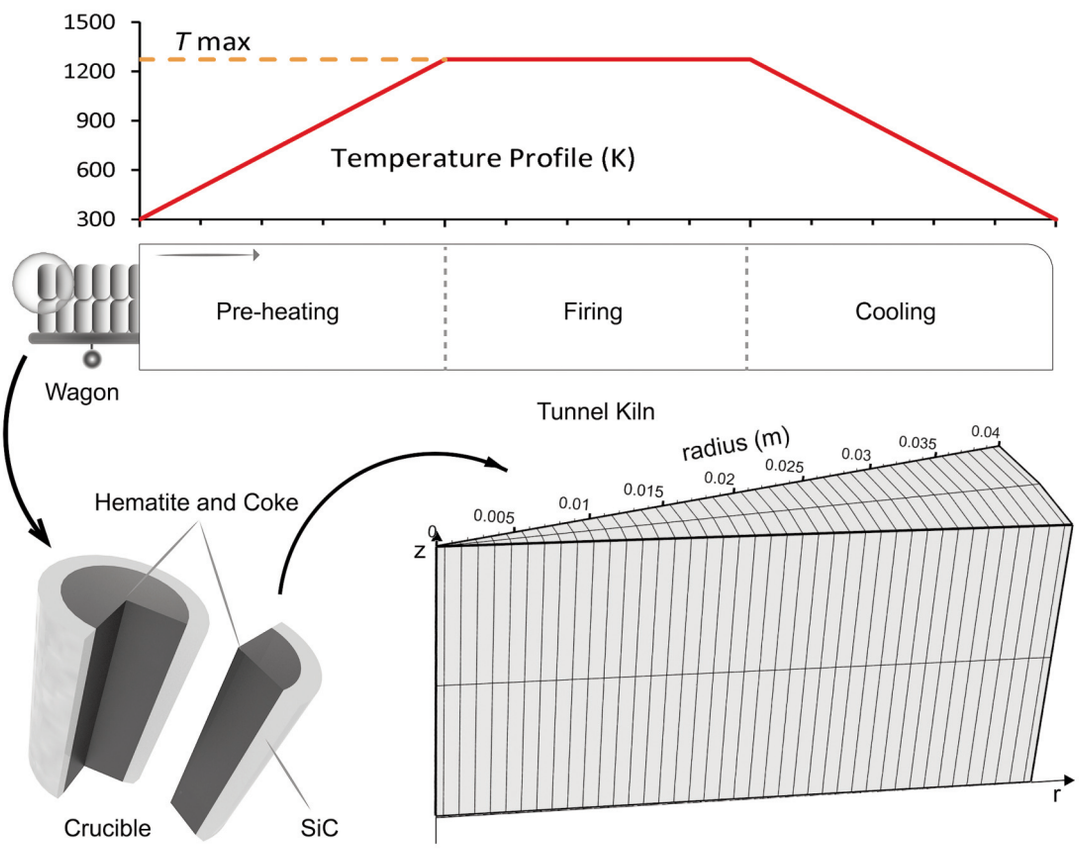

Figure 1. *Schematics of the furnace and the computational domain of the problem*

3.2. Governing Equations

Four dependent variables are to be obtained; the temperature T, and volume fractions of the phases (g_1: gas, g_2: hematite, g_3: magnetite). Accordingly, four governing equations (2) to (5) are proposed; an energy equation, two continuity equations, and a mass balance for the volume fraction of gas.

$$\frac{\partial(\rho c_{\mathrm{p}} T)}{\partial t} = \frac{1}{r}\frac{\partial}{\partial r}\left(r\,k\,\frac{\partial T}{\partial r}\right) \tag{2}$$

$$\frac{\partial\left(g_2\rho_2\right)}{\partial t} = S_2 \quad \text{hematite} \tag{3}$$

$$\frac{\partial\left(g_3\rho_3\right)}{\partial t} = S_3 \quad \text{magnetite} \tag{4}$$

$$\sum_k g_k = 1 \qquad k = 1,2,3 \tag{5}$$

$$S_k = Z_k M_k \left\langle R\right\rangle^V \qquad k = 2,3 \tag{6}$$

$$\left\langle R\right\rangle^V = A_{12}^V\, K_{\mathrm{o}}''\exp\left(-\frac{E_{\mathrm{A}}}{RT}\right)\overline{\rho_{\mathrm{A}}^{-1}}\,C_{\mathrm{A}}^1 \tag{7}$$

Equations (3) and (4) involve interfacial mass transfer rates S_k (kg.m^{-3}s^{-1}) due to the chemical reaction, which is addressed in rate equations (6) involving the volumetric rate of the chemical reaction in $\langle R \rangle^V$(mol.m^{-3}s^{-1}). Equation (7) proposes a modified edition of the volumetric reaction rate explained in the following paragraph.

The kinetics of a heterogeneous reaction is evaluated by $\langle R_A \rangle^i$ in (mol.m^{-2}s^{-1}); an interfacial rate of molar consumption of CO (reactant A), per unit gas-solid interphase area [29]:

$$\langle R_A \rangle^i = \frac{1}{A_{12}}\frac{\partial N_A^1}{\partial t} = \frac{V_1}{A_{12}}\frac{\partial c_A^1}{\partial t} = K''\left(c_A^1\right)^{n_A}\left(c_B^2\right)^{n_B} \quad (8)$$

$$\left(\frac{\text{mol}_A}{\text{m}^2\text{s}}\right) = \left(\frac{1}{\text{m}^2}\right)\frac{(\text{mol}_A)}{(\text{s})} = \left(\frac{\text{m}_1^3}{\text{m}^2}\right)\frac{\left(\frac{\text{mol}_A}{\text{m}_1^3}\right)}{(\text{s})} = \left(\frac{\text{m}}{\text{s}}\right)\left(\frac{\text{mol}_A}{\text{m}_1^3\text{s}}\right)^1\left(\frac{\text{mol}_B}{\text{m}_2^3\text{s}}\right)^0$$

Where A_{12} is the gas-solid interface area (in m^2) and K'' is the heterogeneous rate constant (in m/s) [29]. The sensitivity orders are $n_A = 1$ and $n_B = 0$, since the reduction of hematite is a first-order reaction [15]. The concentrations c_A^1 and c_B^2 can be replaced with the counterpart compositions (C_i^k) according to the relation $c_i^k = \rho_k C_i^k / M_i$ for numerical convenience. From equation (8), the rate of change of concentration of CO in the gaseous phase is obtained:

$$\frac{\partial c_A^1}{\partial t} = \frac{A_{12}}{V_1}K''\left(\frac{\rho_1}{M_A}C_A^1\right) \quad (9)$$

Regarding the CFD routines based on Finite Volume Method, we would rather find the volumetric reaction rate for the continuity equations (3) and track the volume fraction of the species in the system. Thus, the volumetric reaction rate in the control volume can be derived using equation (9):

$$\langle R \rangle^V = \frac{V_1}{V}\frac{1}{Z_A}\left(\frac{\partial c_A^1}{\partial t}\right) = \frac{V_1}{V}\frac{1}{Z_A}\left(\frac{\rho_1}{M_A}\frac{A_{12}}{V_1}K''C_A^1\right) = \frac{g_1\rho_1}{M_A Z_A}A_{12}^V K''C_A^1 \quad (10)$$

Where $A_{12}^V = A_{12}/V$ is the interfacial area density. The extrinsic molar density of the gaseous reactant $\rho_A^{-1} = (g_1\rho_1)/(M_A Z_A)$ in (mol/m^3) appears in RHS of equation (10) and equation (7), consequently. Equations (8) and (10) disclose that the relation between the volumetric reaction rate and the interfacial molar consumption rate is $\langle R \rangle^V = g_1 A_{12}^V \langle R_A \rangle^i / Z_A$. The heterogeneous rate constant K'' is evaluated as:

$$K'' = K_o''\exp\left(-\frac{E_A}{RT}\right) \quad (11)$$

Substituting equation (11) in equation (10) gives equation (7) whereby the model involves the morphological effect A_{12}^V, the thermal effect (the exponential term), and the chemical effects $\rho_A^{-1}C_A^1$, in the kinetics of the heterogeneous reaction. With the morphology term involved separately, the assumption of first-order reaction for the reduction of iron oxide is more reasonable now. From experimental observations [30] the interface area density of the solid phase is in the order of 1000 cm^2/cm^3. The activation energy of 48.70 (kJ/mol) [24] was used in this study. Table 2 lists the parameters used in the current numerical model.

3.3. Boundary conditions

To estimate an effective heat transfer coefficient, an overall heat resistance was evaluated by collecting all heating/cooling effects on the surface of the crucible [34]. From the thermal resistance analogy of the container surface, it was obtained that:

$$R_{\text{total}} = R_{\text{cond}} + \left(R_{\text{conv}}^{-1} + R_{\text{rad}}^{-1}\right)^{-1}$$
$$\left(\frac{1}{2\pi r_2 h_{\text{eff}}}\right) = \left(\frac{\ln(r_1/r_2)}{2\pi k_C}\right) + \left(\left(\frac{1}{2\pi r_2 h_{\text{conv}}}\right)^{-1} + \left(\frac{1}{2\pi r_2 h_{\text{rad}}}\right)^{-1}\right)^{-1} \quad (12)$$

$$h_{\text{eff}} = \frac{k_C}{r_2\ln(r_1/r_2)(h_{\text{conv}} + h_{\text{rad}}) + k_C}\left(h_{\text{conv}} + h_{\text{Rad}}\right) \quad (13)$$

Where $r_1 = r_C$ and $r_2 = r_C + d_C$ are the internal and external radius of the crucible respectively, and $h_{Rad} = \sigma\varepsilon(T + T_{Air})(T^2 + T_{\text{Air}}^2)$ is radiation heat transfer coefficient. The furnace air temperature was calculated from the crucible position (assumption 3). The boundary conditions are summarized in Table 3.

4. Numerical method and testing

A numerical model was developed based on equations (2) to (7) to predict the partial reduction of hematite in the tunnel furnace. Finite-Volume-Method was used to discretize the governing equation. A fully-implicit transient scheme was adopted to promote the stability and speed of calculations with flexible time-steps. Source-term linearization was applied to the continuity sources to obtain a stable numerical model without severe under-relaxation. The numerical model was implemented via a program in FORTRAN based on a CFD code SENSE [35, 36]. Figure 2 shows the algorithm of the numerical calculations. The convergence criteria were set as the maximum relative variation of all dependent variables was less than a small value in the order of 10^{-5}. A grid-dependency study showed that grids smaller than 5 mm and time step less than 2 sec give a fast performance with a discretization error of less than 5% (excluding the error of the assumptions).

The progress of the reaction was quantified by the degree of reduction and the conversion ratio. The degree of reduction α was calculated as the ratio of the released oxygen mass to the initial oxygen mass [14]. The maximum value of α is 0.111, since the reduction of hematite is partial. According to equation (15), the conversion ratio β was calculated as the ratio of

Table 2. *Parameters and properties used in the numerical model*

Parameter	**Value**	**Unit**	**Reference**
Molar masses, M_A, M_B, M_C, M_D	28.01, 159.69, 44.01, 231.53	g/mol	[28, 31]
Densities, ρ_B, ρ_D	5.24, 5.17	g/cm^3	[28, 31, 32]
Specific heat capacity, C_p	570	J.kg^{-1}K^{-1}	[31, 33]
Interface area density, A_{12}^V	1000	cm^2/cm^3	[30]
Frequency constant, K_o	5.58	m/s	[24, 31]
Activation energy, E_A	48.7	kJ/mol	[24, 31]
Furnace length, L	100	m	[20]
Crucible velocity, v_c	1.39	m/min	[20]
Crucible thickness, d_c	4	cm	[20]
Initial CO composition, C_A^1	0.3	-	[31, 32]
Maximum Furnace Temperature, T_F	1273, 1473	K	[32]
Initial hematite porosity, g_1^0	0.3	-	[31, 32]
Case studies	Crucible thickness, d_c(mm)	Crucible radius, R (mm)	
T1	7.5	250	
T2	15	250	
T3	30	250	
R1	15	200	
R3	15	300	

Table 3. *The boundary conditions*

No.	Boundary	Position	Temperature	Volume fraction of the phases		
				Gas	Hematite	Magnetite
0	Initial conditions	$t = 0$	$T_0 = 300\ K$	$g_1 = 0.2$	$g_2 = 0.8$	$g_3 = 0$
1	Crucible center	$r = 0$	$q_r = 0$	$\frac{\partial g_1}{\partial r} = 0$	$\frac{\partial g_2}{\partial r} = 0$	$\frac{\partial g_3}{\partial r} = 0$
2	Crucible wall	$r = r_C$	$q_r = -h_{eff}(T-T_{Air})$ $h_{eff} \approx 200$ (W/m^{2}K)	$\frac{\partial g_1}{\partial r} = 0$	$\frac{\partial g_2}{\partial r} = 0$	$\frac{\partial g_3}{\partial r} = 0$
$T_{Air} = a_j + b_j v_C t$, $T_{Amb} = 300\ K$						
	Furnace air temperature		$a_j = \begin{cases} 0 \\ T_F \\ \frac{LT_F - L_2 T_{Amb}}{L - L_2} \end{cases}$ $b_j = \begin{cases} T_F / L_1 \\ 0 \\ -\frac{T_F - T_{Amb}}{L - L_2} \end{cases}$ $j = \begin{cases} 1 \text{ preheat zone} \\ 2 \text{ firing zone} \\ 3 \text{ cooling zone} \end{cases}$			

converted hematite over the initial hematite:

$$\alpha = \frac{\left[\begin{matrix}\text{Oxygen}\\ \text{in initial}\\ \text{hematite}\end{matrix}\right] - \left[\begin{matrix}\text{Oxygen}\\ \text{in current}\\ \text{Hematite+}\\ \text{Magnetite}\end{matrix}\right]}{\left[\begin{matrix}\text{Oxygen}\\ \text{in initial}\\ \text{Hematite}\end{matrix}\right]} = \frac{3m_B^o - \left(3m_B + 4\frac{Z_B}{Z_D}\left(m_B^o - m_B\right)\right)}{3m_B^o} = \quad (14)$$

$$= \frac{\sum\left(\rho^o f_2^o - \rho f_2\right)}{9\sum \rho^o f_2^o}$$

$$\beta = \frac{\left[\begin{matrix}\text{reduced}\\ \text{hematite}\end{matrix}\right]}{\left[\begin{matrix}\text{initial}\\ \text{hematite}\end{matrix}\right]} = \frac{\frac{-Z_B}{Z_D}\left[\begin{matrix}\text{produced}\\ \text{magnetite}\end{matrix}\right]}{\left[\begin{matrix}\text{initial}\\ \text{hematite}\end{matrix}\right]} = \frac{2}{3}\frac{M_B}{M_D}\frac{\sum \rho f_3}{\sum \rho^o f_2^o} \quad (15)$$

To validate the model, the parameters and properties of the reduction of hematite-to-magnetite published by Donskoi and Mcelwain [31] and Haque, et al. [1] were used (See Table 2). The references have

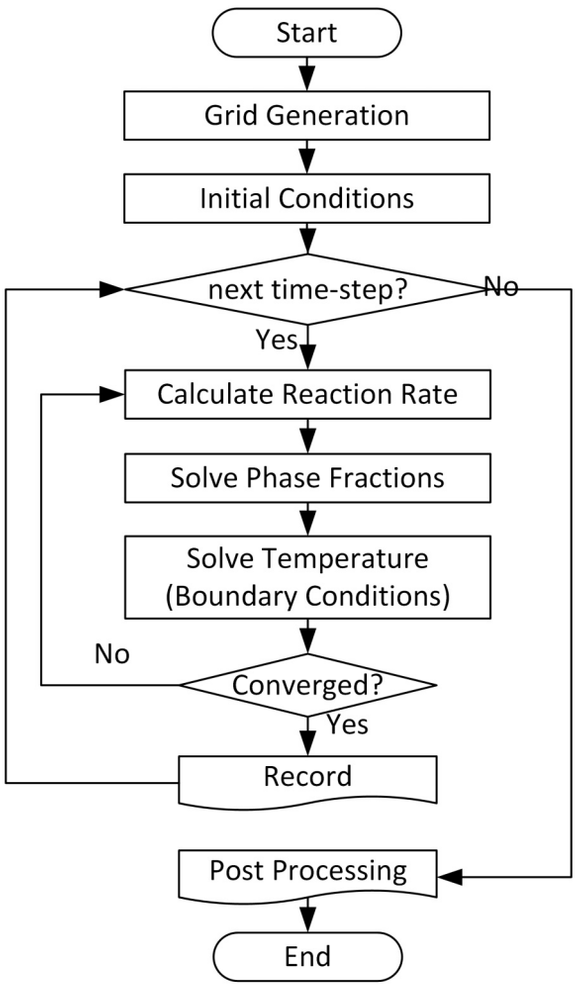

Figure 2. *Numerical solution algorithm*

provided a benchmark test, available with experimental results (Fig 2 of ref. [31] and Fig 15 of ref. [1]), which is suitable for the testing of kinetic models of the reduction of hematite-to-magnetite by carbon monoxide. The numerical setup was then executed using the same parameters and a constant external temperature to simulate the degree of reduction of hematite (alpha) versus time. After the validation of the kinetic model was done, the model was readjusted to simulate the process of the partial reduction of hematite in the tunnel kiln.

5. Results and discussion

Figure 3 shows the predicted degree of reduction of hematite versus the traveling time of the crucible. Decreasing the grid size to 0.5 cm guaranteed that the model was converging toward a unique solution. A similar analysis was done with different time steps and a fully-implicit time-step of $\Delta t = 1$ s was found to be optimally sufficient. The discretization error was evaluated to be less than 5%. Figure 4 displays the degree of reduction at the early stages of the reaction ($\alpha < 0$) which involved only the magnetite formation [32]. The trend and slope of the numerical curve in Figure 4 provided a reasonable prediction for the progression of the reaction. To have an error estimation for the validation of the process model, the standard deviation of the relative difference between numerical and experimental data was calculated; $e_{\text{valid}} = \text{STD}[(y_i^{\text{Num}} - y_i^{\text{Exp}}) / y_i^{\text{Exp}}]$ which yielded ~0.07 or 7% for the results shown in Figure 4. Figure 5 displays

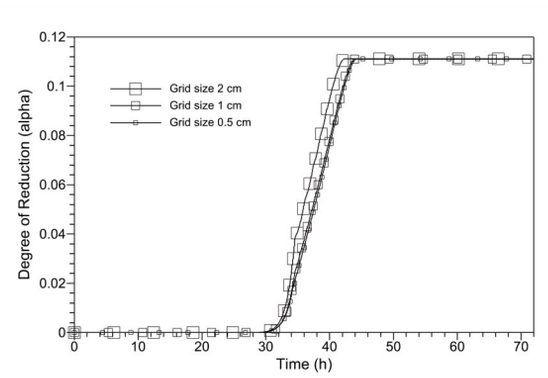

Figure 3. *The degree of reduction of hematite with different grid sizes 0.5 cm, 1 cm, and 2 cm*

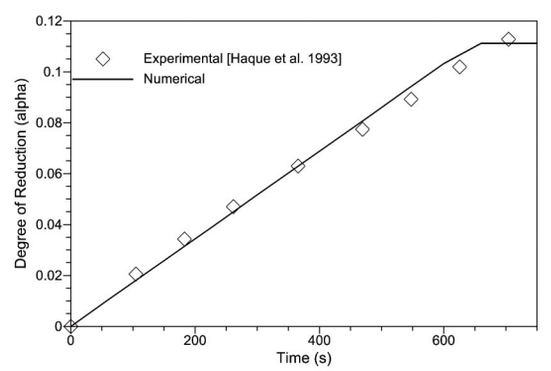

Figure 4. *Calculated degree of reduction in comparison with the experimental results observed by Haque, et al. [1]*

temperature distributions in the crucible at different moments. The temperature profiles indicate that the direct reduction of hematite in the tunnel furnace was a non-isothermal process. Non-uniformity in the temperature profile is significant in the preheating region. Figure 6 shows volume fractions of the constituents in the crucible at different times in the firing region. The hematite fraction started to decrease at the outer radius as soon as the crucible entered the firing region. Remarkably, the volume fraction curves show a step-wise profile with a near steep change in a short distance of 2-3 cm, i.e., the reaction is not predicted to take place everywhere simultaneously. A

distinguishable reaction front is moving from the surface to the center during the process, which concurs well with previous observations by Haghi, et al. [23]. Figure 7 illustrates the computed overall

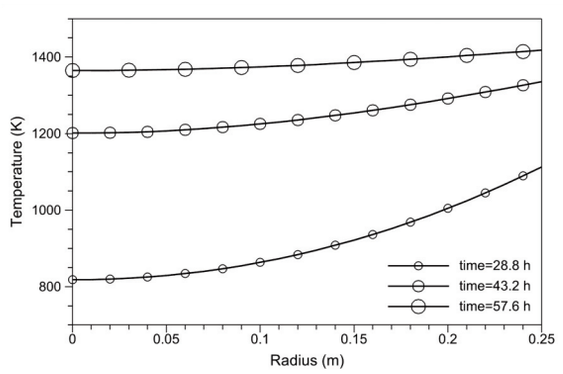

Figure 5. *Temperature distributions in the crucible at the end of furnace regions; (a) at t=28.8 h , (b) at t=43.2 h , (c) at t=47.6 h*

reaction progress. The reaction of hematite-to-magnetite was predicted to start at the beginning of the firing zone. The conversion ratio showed a progression in the first third of the length of the firing zone, which took just about 10 hours to complete the reaction. Since the reduction of hematite-to-magnetite occurred at the initial stages of the iron oxide reduction, the total length of the tunnel kiln would not be necessary for the partial reduction of hematite in the real case. However, to check the numerical model's performance and conduct a parametric study, the final time of the simulations was set to reach the total length of the tunnel kiln. The effect of the crucible's thickness on the progress of the reaction is illustrated in Figure 8 (See Table 2). Although the crucible thickness increased the heat resistance of the wall, it reduced the convective resistance by increasing the surface area. The activation energy of the reaction was supplied from convective heat flow by air on the crucible surface. Consequently, with a 50% decrease in the crucible thickness, the model resulted only in a 1% shift in the occurrence time of the reaction. Then, in small thicknesses, it made just a slight shift at the beginning of the reduction. The crucible thickness could rather be regarded as an economical process parameter, e.g., to improve the durability of crucibles or to reduce the cost of refractory materials. Despite the thickness, the crucible size showed a noteworthy impact on the progress of the reaction. Figure 9 reports the variation of the conversion ratio for three different crucible sizes. Calculations showed that a 20% decrease in the crucible diameter would result in a 10% increase in the overall rate of the reduction. It implies that the crucible's internal heat transfer played a major role in the reduction progress. Any change in the crucible size affected the slope of the overall progression. Then, the process design required a tight correlation between crucible size and wagon speed.

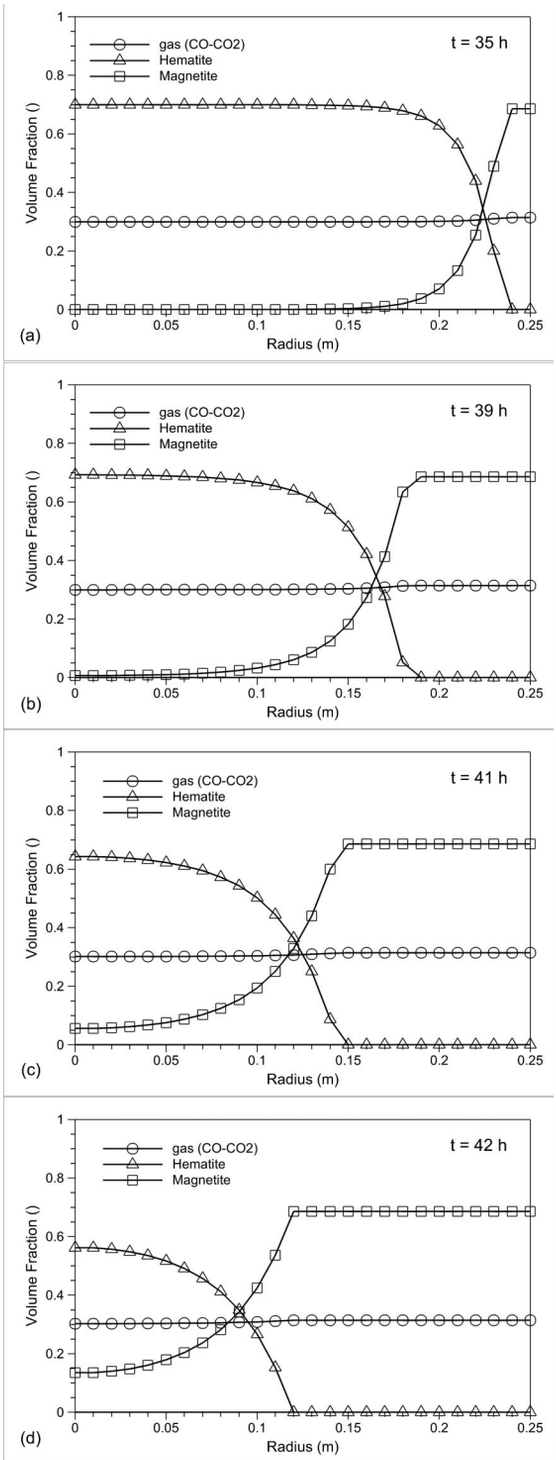

Figure 6. *Numerical volume fraction distributions of hematite, magnetite, and gas phase in the crucible; at (a) t=35 h , (b) t=39 h , (c) t=41 h, and (d) t=42 h*

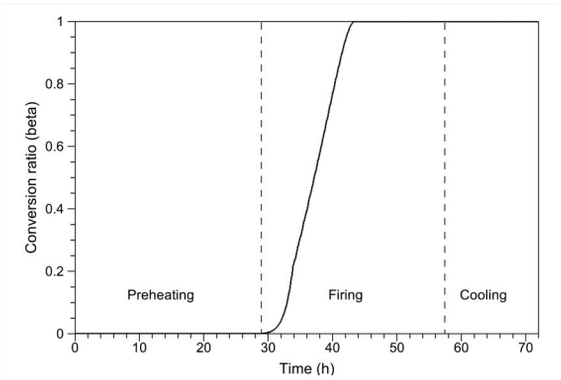

Figure 7. *The predicted overall conversion ratio of the reaction in the tunnel furnace*

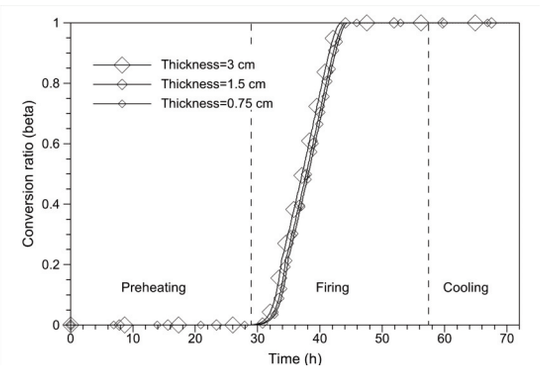

Figure 8. *The overall conversion ratio of the reaction with different crucible thicknesses; Cases T1, T2, and T3*

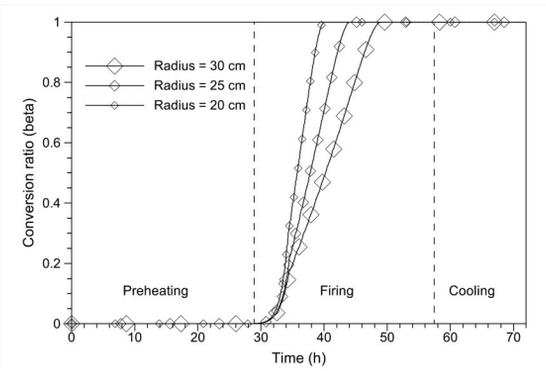

Figure 9. *Overall conversion ratio with different crucible sizes, Cases R1, R2, and T2*

6. Conclusion

A mathematical model was presented to predict the carbothermic partial reduction of hematite in a tunnel furnace crucible. The model consisted of the energy and continuity equations e(2) to (7) with the source terms for species consumption/production rates due to the reaction. The contribution of this model was a modified volumetric reaction rate formulated in equation (7) based on the kinetics of heterogeneous reactions. The following concluding remarks can be drawn:

(1) The volumetric reaction rate in equation (10) introduced an interface area density term, which directly involved the solid morphology effect in the model. This made it possible to exclude the morphological effects from the order of the reaction and the rate constant. Therefore, the first-order reaction became a more realistic assumption.

(2) The model anticipated the distributions of hematite and magnetite (Figure 6) with a step-wise profile and a near steep change in a 2 3 cm distance. This means a distinguishable reaction front was moving from the surface to the center of the crucible throughout the process.

(3) A 50% decrease in the crucible thickness resulted in just a 1% shift at the beginning of the reaction, without any change in the overall rate of the reduction.

(4) Internal heat transfer within the crucible had a serious role in the progress of the reduction of hematite. A 20% decrease in the diameter of the crucible yielded a 10% increase in the reduction process's overall rate (decrease in the duration). Therefore, the process design requires a tight correlation between crucible size and wagon speed.

Acknowledgments

The authors would like to thank Dr. Davoud Haghshenas for his discussions and advice. This research did not receive any grant from public, commercial, or not-for-profit funding agencies. The authors declare that they have no competing interests.

Author's contributions

Author 1. adjusted the code, performed the numerical simulations, and wrote the manuscript. Author 2. developed the theoretical formalism, developed the computational code, and wrote the manuscript. Author 3 revised the manuscript.

Data availability

The authors confirm that the data supporting the findings of this study are available within the article. Details on the numerical simulation are available from the corresponding author upon request.

Conflict of interest

All authors declare that they have no conflicts of interest.

NOMENCLATURE

Letters		**Greek letters**	
A^V	Interface area density (m^2/m^3)	α	Degree of reduction
(C_i^k)	Composition of species *i* in phase *k*	β	Conversion ratio of reaction
c_i^k	Concentration of species *i* in phase *k* (mol/m^3)	ε	Radiation emissivity
c_p	Specific heat capacity ($J.kg^{-1}K^{-1}$)	ρ	Density (kg/m^3)
d_C	Crucible thickness	σ	Stefan-Boltzmann constant
E_A	Activation energy (J/mol)		
f	Mass fraction	**Superscripts**	
g	Volume fraction	i	Interfacial
H	Height (m)	k	Phase index
h	Heat transfer coefficient ($Wm^{-2}K^{-1}$)	o	Initial, old value
K''	Heterogeneous reaction rate constant (m/s)	V	Volumetric
K_O''	Heterogeneous frequency constant (m/s)	**Subscripts**	
k	Thermal conductivity ($Wm^{-1}K^{-1}$)	A	Carbon monoxide
L	Furnace length (m)	B	Hematite
L_1	Furnace preheating length (m)	C	Crucible, carbon dioxide
L_2	Furnace firing length (m)	D	Magnetite
M	Molar mass (kg/mol)	i	Species index
n_i	Order of sensitivity for species	k	Phase index
	Volumetric Reaction rate ($mol.m^{-3}s^{-1}$)	Air	Furnace air
R	Universal gas constant ($J.mol^{-1}K^{-1}$)	Amb	Ambient
r	radius	col	Cooling zone
S_k	Interfacial mass transfer rate ($kg.m^{-3}s^{-1}$)	$cond$	Conduction
T	Temperature (K)	$conv$	Convection
t	Time (s)	eff	Effective value
V	Volume of the representative element (m^3)	fir	Firing zone
v	Velocity (m/s)	pre	Preheating zone
Z	Stoichiometry coefficient	rad	Radiation

References

[1] R. Haque, H.S. Ray, A. Mukherjee, Reduction of iron-ore fines by coal char fines-development of a mathematical-model, Scandinavian Journal of Metallurgy, 21 (1992) 78-85. http://ore.immt.res.in/handle/2018/378

[2] A. Chatterjee, B. Pandey, Metallics for steelmaking: production and use, Allied Publishers, New Delhi, 2001, p.730.

[3] H.Z. Abou-Ziyan, Convective heat transfer from different brick arrangements in tunnel kilns, Applied Thermal Engineering, 24(2-3) (2004) 171-191. https://doi.org/10.1016/j.applthermaleng.2003.08.014

[4] S.A. Hussnain, M. Farooq, M. Amjad, F. Riaz, Z.U.R. Tahir, M. Sultan, I. Hussain, M.A. Shakir, M.A. Qyyum, N. Han, Thermal analysis and energy efficiency improvements in tunnel kiln for sustainable environment, Processes, 9(9) (2021) 1629. https://doi.org/10.3390/pr9091629

[5] F. Abdul, A.B. Anhar, Y. Setiyorini, V.A. Setyowati, S. Pintowantoro, The Role of a mixture of coal and dolomite in the direct reduction process of low-grade iron sand concentrate: a pilot-scale study, Transactions of the Indian Institute of Metals, 75 (2022) 2969-2976.

https://doi.org/10.1007/s12666-022-02685-4

[6] R. Oba, T.S. Possamai,V.P. Nicolau, Thermal analysis of a tunnel kiln used to produce roof tiles, Applied Thermal Engineering, 63(1) (2014) 59-65. https://doi.org/10.1016/j.applthermaleng.2013.10.063

[7] B. Hou, H. Zhang, H. Li, Q. Zhu, Determination of the intrinsic kinetics of iron oxide reduced by carbon monoxide in an isothermal differential micro-packed bed, Chinese Journal of Chemical Engineering, 23(6) (2015) 974-980. https://doi.org/10.1016/j.cjche.2015.01.006

[8] U. Colombo, F. Gazzarrini, G. Lanzavecchia, Mechanisms of iron oxides reduction at temperatures below 400 C, Materials Science and Engineering, 2(3) (1967) 125-135. https://doi.org/10.1016/0025-5416(67)90030-4

[9] W. K. Jozwiak, E. Kaczmarek, T. P. Maniecki, W. Ignaczak,W. Maniukiewicz, Reduction behavior of iron oxides in hydrogen and carbon monoxide atmospheres, Applied Catalysis A: General, 326(1) (2007) 17-27. https://doi.org/10.1016/j.apcata.2007.03.021

[10] K. Piotrowski, K. Mondal, T. Wiltowski, P. Dydo,G. Rizeg, Topochemical approach of kinetics of the reduction of hematite to wüstite, Chemical Engineering Journal, 131(1) (2007) 73-82. https://doi.org/10.1016/j.cej.2006.12.024

[11] A. Pineau, N. Kanari, I. Gaballah, Kinetics of reduction of iron oxides by H2: Part I: Low temperature reduction of hematite, Thermochimica Acta, 447(1) (2006) 89-100. https://doi.org/10.1016/j.tca.2005.10.004

[12] J. P. Gaviria, A. Bohe, A. Pasquevich, D. M. Pasquevich, Hematite to magnetite reduction monitored by Mossbauer spectroscopy and X-ray diffraction, Physica B: Condensed Matter, 389(1) (2007) 198-201.

https://doi.org/10.1016/j.physb.2006.07.056

[13] B. Yu, Dynamic modeling of a tunnel kiln, Heat Transfer Engineering, 15(2) (1994) 39-53. https://doi.org/10.1080/01457639408939823

[14] A. Chatterjee, Sponge iron production by direct reduction of iron oxide, PHI Learning Pvt. Ltd., 2010, p.353.

[15] E. Donskoi, D.L. S. McElwain, L.J. Wibberley, Estimation and modeling of parameters for direct reduction in iron ore/coal composites: Part II. Kinetic parameters, Metallurgical and Materials Transactions B, 34(2) (2003) 255-266. https://doi.org/10.1007/s11663-003-0012-2

[16] E. Donskoi, D.L.S. McElwain, Mathematical modelling of non-isothermal reduction in highly swelling iron ore-coal char composite pellet, Ironmaking & steelmaking, 28(5) (2001) 384-389. https://doi.org/10.1179/irs.2001.28.5.384

[17] C.E. Seaton, J.S. Foster, J. Velasco, Reduction kinetics of hematite and magnetite pellets containing coal char, Transactions of the Iron and Steel Institute of Japan, 23(6) (1983) 490-496. https://doi.org/10.2355/isijinternational1966.23.490

[18] G.F. Gao, X.L. Zhou, Z. Shi, L.P. Liu, Study on the kinetics of gas-solid based synergistic reduction of limonite carbon-containing pellets, Journal of Mining and Metallurgy, Section B: Metallurgy, 57(2) (2021) 185-193. https://doi.org/10.2298/JMMB200510017G

[19] S. Pintowantoro, F. Abdul, F. Sanubari, Study of the effect of binder types on the reduction process and metallurgical properties of Indonesian titanomagnetite iron sand in the point of view of tunnel kiln process, Journal of Chemical Technology and Metallurgy, 56(1) (2021) 227-234. https://www.scopus.com/inward/record.url?eid=2-s2.0-85098736040&partnerID=MN8TOARS

[20] S.C. Khattoi, G.G. Roy, Reduction efficiency of iron ore–coal composite pellets in tunnel kiln for sponge iron production, Transactions of the Indian Institute of Metals, 68(5) (2015) 683-692. https://doi.org/10.1007/s12666-014-0498-0

[21] F. Abdul, S. Pintowantoro, A.B. Hidayatullah, Analysis of cylindrical briquette dimension on total iron content and the degree of metallization in direct reduction process of iron ore and iron sand mixture, Materials Science Forum, 964 (2019) 19-25. https://doi.org/10.4028/www.scientific.net/MSF.964.19

[22] S. Saleem, S. Mishra, G. G. Roy, A simulation study of reduction kinetics for sponge iron production in a rotary hearth furnace, Canadian Metallurgical Quarterly, 59(2) (2020) 180-188. https://doi.org/10.1080/00084433.2020.1730117

[23] S. M. A. Haghi, A. Zabett, M. Mirjalili, Mechanism of reduction of hematite-magnetite hollow cylindrical pellet by graphite-calcium carbonate mixture, Metallurgical and Materials Transactions B, 51(4) (2020) 1460-1468. https://doi.org/10.1007/s11663-020-01852-6

[24] J. Yu, Y. Han, Y. Li, P. Gao, W. Li, Mechanism and kinetics of the reduction of hematite to magnetite with CO–CO2 in a micro-fluidized bed, Minerals, 7(209) (2017) 1-12. https://doi.org/10.3390/min7110209

[25] M. S. Valipour, Mathematical modeling of a non-catalytic gas-solid reaction: hematite pellet reduction with syngas, Scientia Iranica, 16(2) (2009) 108-124. https://scientiairanica.sharif.edu/article_3274.html

[26] V. Kumari, G. G. Roy, P. K. Sen, Mathematical model to estimate the rate parameters and thermal efficiency for the reduction of iron ore–coal composite pellets in multi-layer bed at rotary hearth furnace, Transactions of the Indian Institute of Metals, 68(1) (2015) 109-116. https://doi.org/10.1007/s12666-014-0434-3

[27] D.R. Gaskell, D.E. Laughlin, Introduction to the thermodynamics of materials, 6th ed., CRC press, Boca Raton, 2017, p.714.

[28] A. Ghosh, A. Chatterjee, Iron making and steelmaking: theory and practice, PHI Learning Pvt. Ltd., New Delhi, 2008, p.472.

[29] O. Levenspiel, Chemical reaction engineering, 3 ed., John Wiley & Sons, New York, 1999, p.668.

[30] L. v. Bogdandy, H. Engell, The reduction of iron ores: scientific basis and technology, Springer-Verlag Berlin Heidelberg GmbH, Dusseldorf, 1971, p.576.

[31] E. Donskoi, D. L. S. McElwain, Estimation and modeling of parameters for direct reduction in iron ore/coal composites: Part I. Physical parameters, Metallurgical and Materials Transactions B, 34(1) (2003) 93-102. https://doi.org/10.1007/s11663-003-0059-0

[32] S.P. Trushenski, K.Li, W.O. Philbrook, Non-topochemical reduction of iron oxides, Metallurgical Transactions, 5(5) (1974) 1149-1158. https://doi.org/10.1007/BF02644326

[33] A. Santos, F. Almeida, F. Rocha, Physical and thermal

properties analysis of hematite for thermal heat storage, Materials, 15(13) (2022) 4846. https://doi.org/10.3390/ma15134648

[34] T.L. Bergman, A.S. Lavine, F.P. Incropera, D.P. Dewitt, Fundamentals of heat and mass transfer, 7th ed., John Wiley & Sons, USA, 2011, p.1048.

[35] A. Jafari, S.H. Seyedein, M.R. Aboutalebi, Semi-implicit method for thermodynamically linked equations in phase change problems (SIMTLE), Applied Mathematical Modelling, 35 (2011) 4774-4789. https://doi.org/10.1016/j.apm.2011.03.051

[36] A. Jafari-Ramiani, Phase change modelling with flexible source-based kinetics for non-equilibrium transitions, International Journal of Thermal Sciences, 159 (2021) 106608. https://doi.org/10.1016/j.ijthermalsci.2020.106608

MODELIRANJE PARCIJALNE REDUKCIJE HEMATITA SA UGLJEN-MONOKSIDOM U TUNELSKOJ PEĆI

S. Salimibani, A. Jafari-Ramiani, S. Firoozi

Politehnički univerzitet u Teheranu, Fakultet za materijale i metalurško inženjerstvo, Teheran, Iran

Apstrakt

Direktna redukcija gvožđa u tunelskoj peći u nekim slučajevima ne dostiže potpuni stepen redukcije. Da bi se rešio problem sa heterogenom brzinom reakcije, kao i sa prenosom toplote i morfologijom oksida potrebno je osmisliti odgovarajući model. U ovom radu se predlaže korišćenje trofaznog modela zasnovanog na očuvanju toplote i mase i kinetici reakcije, kako bi se opisala redukcija hematita u magnetit u loncu za topljenje. Fortran program je korišćen za primenu modela gde se koristila diskretizacija konačnog obima, a rezutati su potvrđeni na osnovu dostupnih eksperimentalnih podataka. Model je doprineo smanjenju nepouzdanosti kod brzine reakcije reformulacijom uzimajući u obzir čvrstu morfologiju. Rezultati su takođe pokazali da brzina, kao i prečnik lonca za topljenje imaju dominantan uticaj na celokupni tok redukcije kada se promeni brzina prenosa toplote unutar lonca. Nasuprot tome, debljina lonca ima manji uticaj na reakciju i može se smatrati ekonomskim parametrom.

Ključne reči: *Modeliranje višefaznih sistema; Hematit; Direktna redukcija; Kinetika; Proizvodnja gvožđa*